

# Asymmetric Metal/ $\alpha$ -In<sub>2</sub>Se<sub>3</sub>/Si Crossbar Ferroelectric Semiconductor Junction

Mengwei Si, Zhuocheng Zhang, Sou-Chi Chang, Nazila Haratipour, Dongqi Zheng, Junkang Li, Uygur E. Avci, and Peide D. Ye\*



Cite This: *ACS Nano* 2021, 15, 5689–5695



Read Online

ACCESS |



Metrics & More



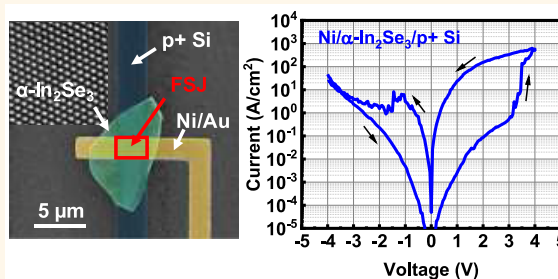
Article Recommendations



Supporting Information

**ABSTRACT:** A ferroelectric semiconductor junction is a promising two-terminal ferroelectric device for nonvolatile memory and neuromorphic computing applications. In this work, we propose and report the experimental demonstration of asymmetric metal/ $\alpha$ -In<sub>2</sub>Se<sub>3</sub>/Si crossbar ferroelectric semiconductor junctions (c-FSJ). The depletion in doped Si is used to enhance the modulation of the effective Schottky barrier height through the ferroelectric polarization. A high-performance  $\alpha$ -In<sub>2</sub>Se<sub>3</sub> c-FSJ is achieved with a high on/off ratio  $> 10^4$  at room temperature, on/off ratio  $> 10^3$  at an elevated temperature of 140 °C, retention  $> 10^4$  s, and endurance  $> 10^6$  cycles. The on/off ratio of the  $\alpha$ -In<sub>2</sub>Se<sub>3</sub> asymmetric FSJs can be further enhanced to  $> 10^8$  by introducing a metal/ $\alpha$ -In<sub>2</sub>Se<sub>3</sub>/insulator/metal structure.

**KEYWORDS:** ferroelectric semiconductor,  $\alpha$ -In<sub>2</sub>Se<sub>3</sub>, asymmetry, nonvolatile memory, 2D material



Emerging nonvolatile memories (e-NVMs) are considered as promising devices for next-generation memory technology and non-von Neumann computing applications. The crossbar array structure is commonly implemented to maximize the cell density in these e-NVMs, such as resistive random-access memory (RRAM),<sup>1,2</sup> phase change memory (PCM),<sup>3</sup> and ferroelectric tunneling junction (FTJ).<sup>4–11</sup> However, there are limitations for these technologies. A FTJ is known to have a relatively low current density because of the tunneling-based electron transport mechanism and challenges in realizing ultrathin ferroelectric films in nanometer scale. The depolarization field is well known to increase while reducing the thickness of a ferroelectric film, resulting in the challenges to realize devices with high polarization stability using an ultrathin ferroelectric film.<sup>12–15</sup> RRAM and PCM may suffer from high power consumption in scaled and high-density devices due to the filament-based conducting mechanism<sup>1</sup> and high programming current density.<sup>3</sup> Their currents also drift with time, leading to the instability of resistance states, especially unfavorable for neuromorphic computing applications.<sup>3</sup>

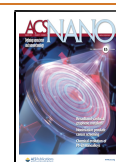
Recently demonstrated ferroelectric semiconductor based two-terminal devices<sup>16,17</sup> such as a crossbar ferroelectric semiconductor junction (c-FSJ)<sup>17</sup> may potentially overcome these challenges. First, the c-FSJ does not require an ultrathin ferroelectric film like in the conventional FTJ because of the combination of ferroelectricity and a semiconducting property in the same material. Carrier transport through a thick ferroelectric film is possible due to the semiconducting

property. On the other hand, the current in a c-FSJ can scale with area because the current transport mechanism is the electron thermionic emission across the Schottky barrier.<sup>17</sup> Therefore, a c-FSJ is promising for high-density and low-power applications. Meanwhile, ferroelectric devices are one of the promising synaptic device candidates for neuromorphic computing because of the multidomain nature of ferroelectric materials.<sup>17–19</sup> It is of great interest to explore ferroelectric material based nonvolatile two-terminal junction devices, such as the FTJ and the c-FSJ studied in this work. Here, 2D ferroelectric semiconductor  $\alpha$ -In<sub>2</sub>Se<sub>3</sub> is used in the c-FSJ.  $\alpha$ -In<sub>2</sub>Se<sub>3</sub> as the channel of a ferroelectric semiconductor field-effect transistor (FeS-FET) was experimentally demonstrated.<sup>20</sup>  $\alpha$ -In<sub>2</sub>Se<sub>3</sub> has a layered non-centrosymmetric rhombohedral *R3m* structure,<sup>21,25</sup> and the non-centrosymmetric crystal structure is the origin of the spontaneous polarization and ferroelectricity.  $\alpha$ -In<sub>2</sub>Se<sub>3</sub> was identified as the ferroelectric semiconductor for the c-FSJ because of its small bandgap of  $\sim 1.39$  eV, room-temperature ferroelectricity with high Curie temperature, and the ability to maintain ferroelectricity down

**Received:** February 1, 2021

**Accepted:** March 1, 2021

**Published:** March 2, 2021



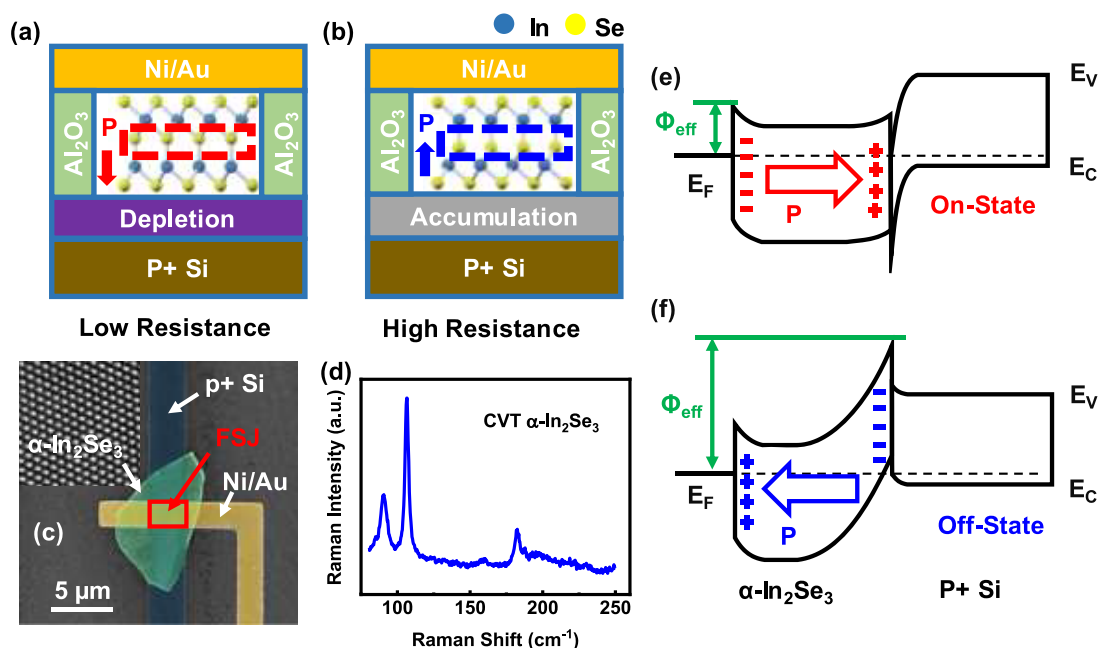


Figure 1. Illustration of the  $\alpha$ - $\text{In}_2\text{Se}_3$  asymmetric c-FSJ at the (a) on-state and (b) off-state. (c) False-colored SEM image of a fabricated  $\alpha$ - $\text{In}_2\text{Se}_3$  asymmetric c-FSJ. The inset image is a high-resolution STEM image of the  $\alpha$ - $\text{In}_2\text{Se}_3$  surface. (d) Raman spectrum of a CVT-grown  $\alpha$ - $\text{In}_2\text{Se}_3$  thin film. Band diagram of the  $\alpha$ - $\text{In}_2\text{Se}_3$  asymmetric c-FSJ at the (e) on-state and (f) off-state.

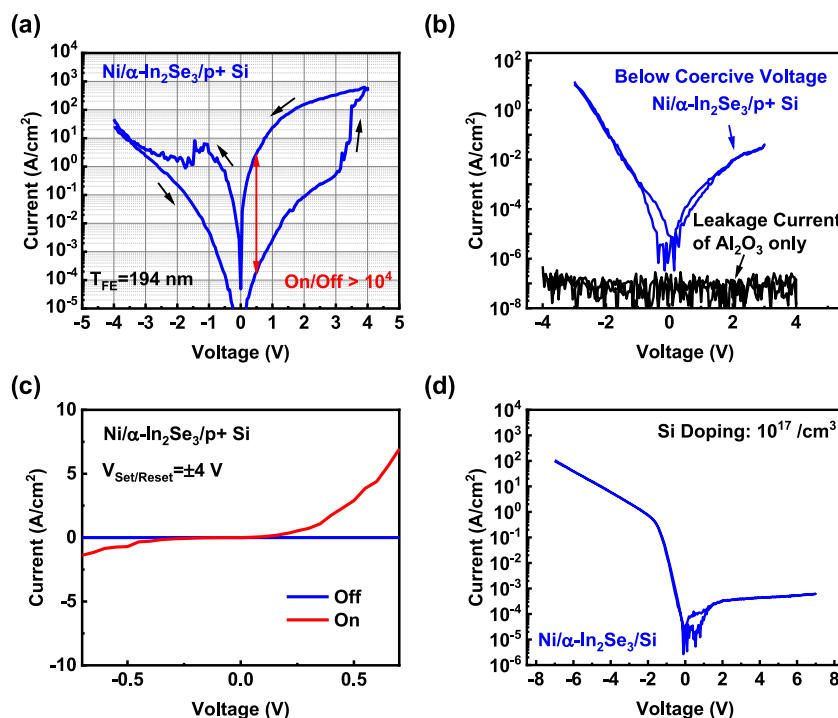
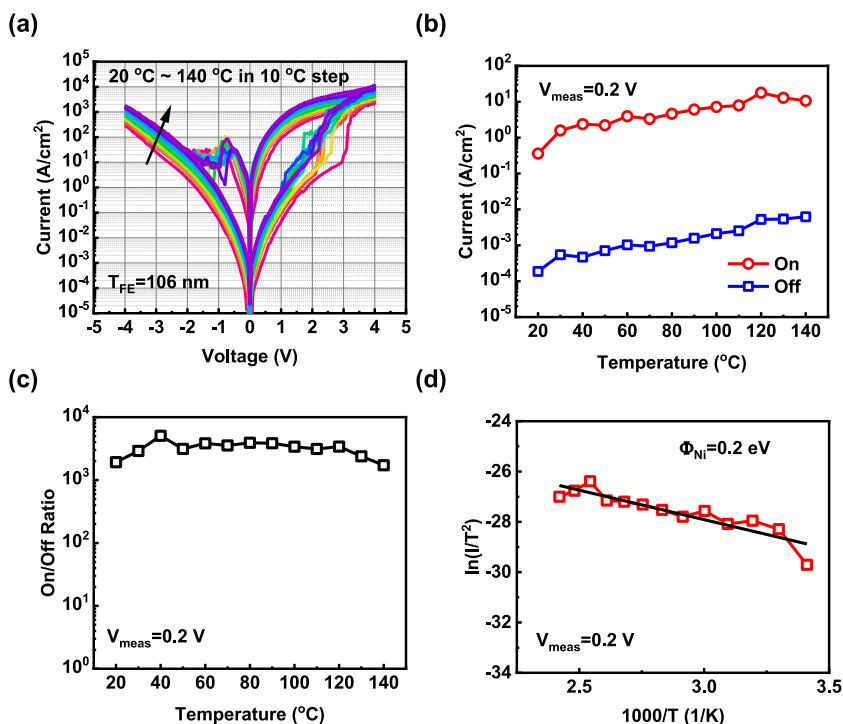


Figure 2. (a)  $I$ - $V$  characteristics of a typical  $\alpha$ - $\text{In}_2\text{Se}_3$  asymmetric c-FSJ, showing an on/off ratio over  $10^4$ . (b)  $I$ - $V$  characteristics with a voltage sweep below the coercive voltage of the same device without ferroelectric switching. The leakage current of the 15 nm  $\text{Al}_2\text{O}_3$  barrier is negligible compared to the current through an  $\alpha$ - $\text{In}_2\text{Se}_3$  asymmetric c-FSJ. (c)  $I$ - $V$  characteristics in linear scale of the same device where the set/reset voltages are  $\pm 4$  V. (d)  $I$ - $V$  characteristics of an  $\alpha$ - $\text{In}_2\text{Se}_3$  asymmetric c-FSJ with a low boron doping of  $10^{17}/\text{cm}^3$  on a silicon electrode, exhibiting a typical p-n junction behavior.

to a few atomic layers.<sup>16,17,20–26</sup> A symmetric metal/ $\alpha$ - $\text{In}_2\text{Se}_3$ /metal c-FSJ was demonstrated with clear ferroelectric resistive switching but with a relatively low on/off ratio around 55 at 0.2 V.<sup>17</sup>

Asymmetric electrodes are commonly applied to enhance the on/off ratio of the FTJ.<sup>8,9,11</sup> In this work, we propose and

experimentally demonstrate an asymmetric metal/ $\alpha$ - $\text{In}_2\text{Se}_3$ /Si c-FSJ. Heavily boron-doped silicon (p+ Si) is used as the bottom electrode. The depletion region in doped Si provides essential asymmetry to the band alignments in the metal/ $\alpha$ - $\text{In}_2\text{Se}_3$ /Si structure, which can enhance the modulation of the effective Schottky barrier height ( $\Phi_{\text{eff}}$ ) by the out-of-plane



**Figure 3.** (a) Temperature-dependent  $I$ – $V$  characteristics of an  $\alpha$ - $\text{In}_2\text{Se}_3$  asymmetric c-FSJ. (b) Current versus temperature at the on-state and off-state of the device, measured at 0.2 V. (c) Temperature-dependent on/off ratio of the device at 0.2 V. (d) Extraction of Schottky barrier height at the on-state from the temperature-dependent  $I$ – $V$  measurement.

ferroelectric polarization. A high-performance  $\alpha$ - $\text{In}_2\text{Se}_3$  c-FSJ is achieved with a high on/off ratio  $> 10^4$  at room temperature, on/off ratio  $> 10^3$  at an elevated temperature of 140 °C, on/off ratio  $> 10^3$  after  $10^4$  s retention measurement, and on/off ratio  $> 10^2$  after  $10^6$  endurance cycles. The on/off ratio of the  $\alpha$ - $\text{In}_2\text{Se}_3$  asymmetric c-FSJ can be further enhanced to  $> 10^8$  by introducing an asymmetric metal/ $\alpha$ - $\text{In}_2\text{Se}_3$ /insulator/metal structure.

## RESULTS AND DISCUSSION

**Figure 1** shows a schematic illustration of the  $\alpha$ - $\text{In}_2\text{Se}_3$  asymmetric c-FSJ at the (a) on-state and (b) off-state. The resistance and band alignments of the device are controlled by the ferroelectric polarization in  $\alpha$ - $\text{In}_2\text{Se}_3$ . The experimental device consists of heavily boron-doped Si (p+ Si, resistivity  $< 0.005 \, \Omega\cdot\text{cm}$ , doping concentration  $\sim 2 \times 10^{19} \, \text{cm}^{-2}$ ) as the bottom electrode and Ni as the top electrode. As the insulating barrier, 15 nm  $\text{Al}_2\text{O}_3$  is used to isolate the top and bottom electrodes. **Figure 1(c)** shows the false-colored SEM image of a fabricated  $\alpha$ - $\text{In}_2\text{Se}_3$  asymmetric c-FSJ, capturing the Ni/Au top electrode, p+ Si bottom electrode, and the  $\alpha$ - $\text{In}_2\text{Se}_3$  flake. The inset image of **Figure 1(c)** is a high-resolution STEM image of the  $\alpha$ - $\text{In}_2\text{Se}_3$  surface, showing the hexagonal crystal structure and highly single-crystallized material. **Figure 1(d)** shows the Raman spectrum of the exfoliated CVT  $\alpha$ - $\text{In}_2\text{Se}_3$  thin film. The Raman shift peak positions confirm its alpha phase.<sup>20</sup>

**Figure 1(e)** and (f) show the band diagram of the  $\alpha$ - $\text{In}_2\text{Se}_3$  asymmetric c-FSJ at the on-state and off-state. In the on-state,  $\alpha$ - $\text{In}_2\text{Se}_3$  is in the polarization down position so that a depletion region is formed at the  $\alpha$ - $\text{In}_2\text{Se}_3$ /Si interface, leading to a lower  $\Phi_{\text{eff}}$  as also illustrated in **Figure 1(a)**. In the off-state,  $\alpha$ - $\text{In}_2\text{Se}_3$  is in a polarization up position, and an accumulation region is formed on Si at the  $\alpha$ - $\text{In}_2\text{Se}_3$ /Si interface, resulting in a higher  $\Phi_{\text{eff}}$  for electrons, as also

illustrated in **Figure 1(b)**. Note that in the off-state, a depletion region in  $\alpha$ - $\text{In}_2\text{Se}_3$  is formed near the  $\alpha$ - $\text{In}_2\text{Se}_3$ /Si interface with low electron density so that resistance is high (high barrier effectively). As can be seen clearly, the band bending in p+ Si contributes to the effective modulation of  $\Phi_{\text{eff}}$  in the on- and off-states. In the  $\alpha$ - $\text{In}_2\text{Se}_3$  symmetric c-FSJ using metal for both the top and bottom electrodes,<sup>17</sup> the modulation of  $\Phi_{\text{eff}}$  is much weaker because of the short screening length in the metal. Note that, in an ideal  $\text{In}_2\text{Se}_3$  symmetric c-FSJ with metal/ $\alpha$ - $\text{In}_2\text{Se}_3$ /metal structure, if it is assumed that two metal electrodes are identical and conductivity is infinitely high, there is no on/off ratio in such devices because all ferroelectric polarization is compensated by the charges in the electrodes. The weak on/off ratio in experimental Ni/ $\alpha$ - $\text{In}_2\text{Se}_3$ /Ni symmetric c-FSJs is because of the asymmetry introduced by the device fabrication process and the existence of the screening length in the metal. Therefore, a larger on/off ratio can be obtained in this  $\alpha$ - $\text{In}_2\text{Se}_3$  asymmetric c-FSJ than in the  $\alpha$ - $\text{In}_2\text{Se}_3$  symmetric c-FSJ.

**Figure 2(a)** shows the  $I$ – $V$  characteristics of a representative  $\alpha$ - $\text{In}_2\text{Se}_3$  asymmetric c-FSJ with a thickness of  $\alpha$ - $\text{In}_2\text{Se}_3$  ( $T_{\text{FE}}$ ) of 194 nm. The double-sweep  $I$ – $V$  curve is measured in a voltage range of  $\pm 4$  V. The ferroelectric resistive switching up and down is clearly observed, showing a high on/off ratio of  $1.5 \times 10^4$  at 0.2 V. The on/off ratios of a metal/ $\alpha$ - $\text{In}_2\text{Se}_3$ /Si c-FSJ at a voltage range from 0.05 to 0.5 V are similar to the on/off ratio at 0.2 V. Therefore, 0.2 V is chosen in the characterization of  $I_{\text{ON}}$ ,  $I_{\text{OFF}}$ , and on/off ratio properties as a representative measurement of voltage ( $V_{\text{meas}}$ ). The on/off ratio of this  $\alpha$ - $\text{In}_2\text{Se}_3$  asymmetric c-FSJ is significantly higher than the previously reported  $\alpha$ - $\text{In}_2\text{Se}_3$  symmetric c-FSJ ( $\sim 55$  at 0.2 V),<sup>17</sup> because of the better modulation of  $\Phi_{\text{eff}}$ , as also discussed in **Figure 1(e)** and (f). Note that the  $T_{\text{FE}}$  here is above 100 nm, which is significantly larger than those in

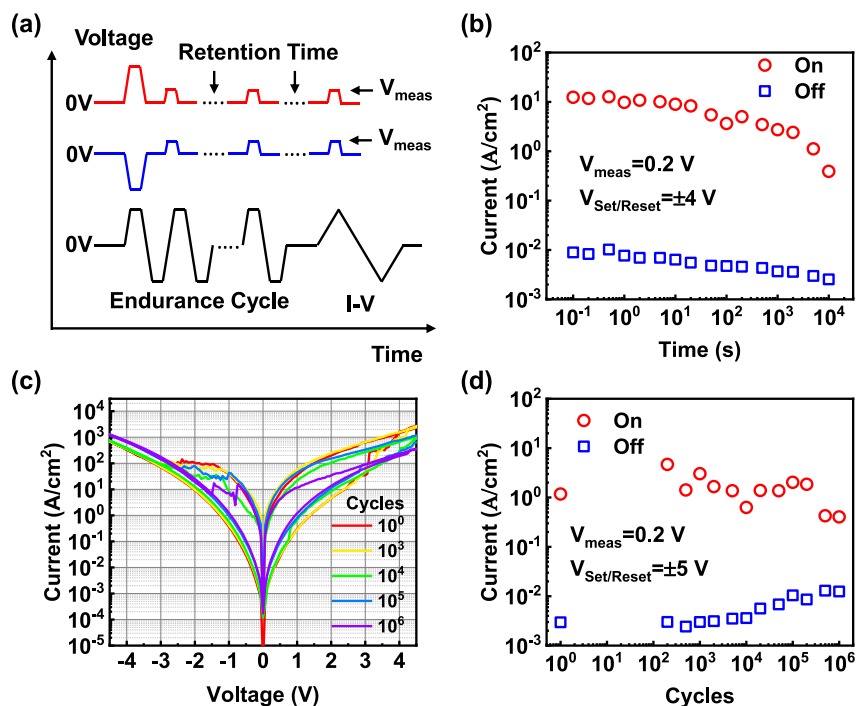


**Figure 4.** (a) Voltage pulse scheme in retention and endurance measurements. (b) Retention characteristics of an  $\alpha\text{-In}_2\text{Se}_3$  asymmetric c-FSJ with  $V_{\text{Set/Reset}} = \pm 4$  V and  $V_{\text{meas}} = 0.2$  V. (c)  $I$ – $V$  characteristics of an  $\alpha\text{-In}_2\text{Se}_3$  asymmetric c-FSJ during endurance measurement with  $V_{\text{Set/Reset}} = \pm 5$  V up to  $10^6$  cycles. (d) Endurance characteristics of the device shown in (c), extracted at 0.2 V.

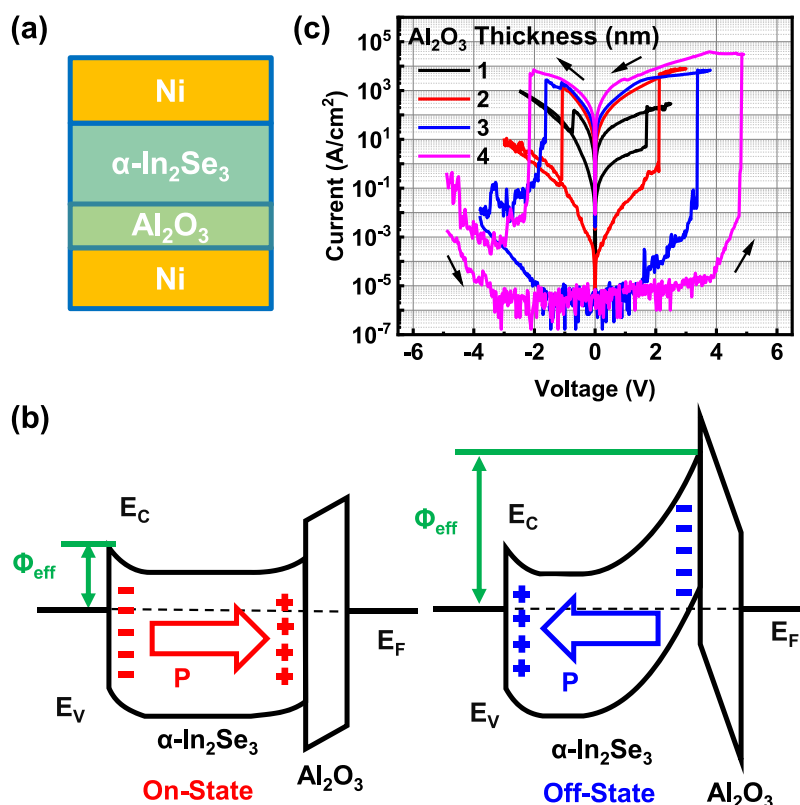
conventional FTJs (at most a few nanometers<sup>9</sup>). This is because the semiconducting nature of  $\alpha\text{-In}_2\text{Se}_3$  allows carriers to transport through the thick ferroelectric film. It is well known that realizing strong ferroelectricity and high polarization stability in ultrathin ferroelectric films is difficult, making it harder to implement high-performance FTJ devices. The proposed asymmetric c-FSJ here can alternatively use a thick ferroelectric film, which is a key advantage of using this c-FSJ over conventional FTJs for low-power two-terminal nonvolatile memory and synaptic device applications. Figure 2(b) illustrates the  $I$ – $V$  characteristics of the same device measured in the  $\pm 3$  V range below the coercive voltage, exhibiting negligible hysteresis without ferroelectric polarization switching. The leakage current through the 15 nm  $\text{Al}_2\text{O}_3$  is negligible. Figure 2(c) presents the  $I$ – $V$  characteristics in linear scale of the same device as in Figure 2(a), where the set/reset voltages ( $V_{\text{Set/Reset}}$ ) are  $\pm 4$  V. The on-state  $I$ – $V$  curve is nonlinear, indicating the current transport mechanism at the on-state is the electron thermal emission across the Schottky barrier instead of a conductance filament like in RRAM. The  $\text{Ni}/\alpha\text{-In}_2\text{Se}_3/\text{p}^+\text{Si}$  asymmetric structure achieved more than 2 orders of magnitude improvement in on/off ratio compared to the  $\text{Ni}/\alpha\text{-In}_2\text{Se}_3/\text{Ni}$  symmetric structure.<sup>17</sup> The improvement mostly benefited from the reduction of the off-current ( $I_{\text{OFF}}$ ) due to a more effective modulation of  $\Phi_{\text{eff}}$ . Optimization of Si substrate doping may contribute to further performance benefits. The  $\alpha\text{-In}_2\text{Se}_3$  asymmetric c-FSJ is almost wake-up free (Figure S1).  $\alpha\text{-In}_2\text{Se}_3$  asymmetric c-FSJ also exhibit no clear thickness dependence on coercive voltages (Figure S2), indicating the polarization switching is a surface-initiated effect due to the nonlinear band bending of the semiconductor.<sup>17</sup> This property is fundamentally different from an FTJ.

Figure 3(a) shows the temperature-dependent  $I$ – $V$  characteristics of an  $\alpha\text{-In}_2\text{Se}_3$  asymmetric c-FSJ with  $T_{\text{FE}} = 106$  nm,

from 20 to 140 °C in 10 °C steps. The ferroelectric resistive switching is clearly observed on all temperatures. The current density increase is due to a thermal current increase, so there is no clear temperature dependence on the coercive voltages, suggesting the Curie temperature of  $\alpha\text{-In}_2\text{Se}_3$  is much larger than 140 °C. Figure 3(b) shows current density versus temperature at on- and off-states at a measurement voltage of 0.2 V. Both on- and off-state currents increase with a temperature increase as a result of electron thermionic emission. This further confirms the transport mechanism of the c-FSJ is the modulation of the effective Schottky barrier by ferroelectric polarization. The device maintains a high on/off ratio of over  $10^3$  and no obvious on/off ratio degradation up to 140 °C, as illustrated in on/off ratio versus temperature characteristics in Figure 3(c), suggesting the  $\alpha\text{-In}_2\text{Se}_3$  c-FSJ has the potential for nonvolatile memory device applications in high-temperature harsh environments. The  $\text{Ni}/\alpha\text{-In}_2\text{Se}_3$  Schottky barrier height ( $\Phi_{\text{Ni}}$ ) is determined by the temperature-dependent measurement at the on-state. According to the current transport equation of the metal/semiconductor junction,<sup>27</sup> where  $I \propto T^2 \exp(q\Phi_{\text{Ni}}/k_{\text{B}}T)$  at a constant applied voltage (0.2 V applied here),  $\ln(I/T^2)$  is in a linear relation with  $1/T$ . Here,  $T$  is temperature,  $q$  is the elementary charge, and  $k_{\text{B}}$  is the Boltzmann constant. Thus,  $\Phi_{\text{Ni}}$  can be extracted from the slope of  $\ln(I/T^2)$  versus  $1/T$ , as shown in Figure 3(d), where the extracted  $\Phi_{\text{Ni}}$  is 0.2 eV. The relatively small electron  $\Phi_{\text{Ni}}$  is consistent with the n-type transistor operation as previously reported.<sup>20</sup>

The retention and endurance are important characteristics of a nonvolatile memory device. However, the retention and endurance characteristics have not been reported on the out-of-plane polarization of the  $\alpha\text{-In}_2\text{Se}_3$  and  $\alpha\text{-In}_2\text{Se}_3$  c-FSJ. Here, the retention and endurance of the  $\alpha\text{-In}_2\text{Se}_3$  asymmetric c-FSJ are studied. The retention measurement is done by applying a





**Figure 5.** (a) Schematic diagram of the asymmetric metal/ $\alpha$ -In<sub>2</sub>Se<sub>3</sub>/insulator/metal c-FSJ. (b) Illustration of the band diagram at the on- and off-state. (c)  $I$ – $V$  characteristics of  $\alpha$ -In<sub>2</sub>Se<sub>3</sub> c-FSJ with different Al<sub>2</sub>O<sub>3</sub> interfacial layer thicknesses. The thicknesses of In<sub>2</sub>Se<sub>3</sub> are 160/250/220/110 nm for devices with 1/2/3/4 nm of Al<sub>2</sub>O<sub>3</sub>, respectively.

set/reset voltage pulse at  $V_{\text{Set/Reset}}$  then measuring the current density at a given  $V_{\text{meas}}$  after a certain amount of retention time as shown in the voltage pulse scheme of retention measurements in Figure 4(a). Figure 4(b) shows the retention characteristics of this device with  $V_{\text{Set/Reset}} = \pm 4$  V,  $V_{\text{meas}} = 0.2$  V, and a set/reset pulse width ( $T_{\text{Set/Reset}}$ ) of 10 ms. A high on/off ratio after  $10^4$  s retention is achieved, suggesting high polarization stability in the c-FSJ. The endurance measurement is done by applying set and reset voltage pulses cyclically at  $V_{\text{Set/Reset}}$  for a given cycle number, then measuring the  $I$ – $V$  characteristics of the device, as shown in the voltage pulse scheme in Figure 4(a). Figure 4(c) shows the  $I$ – $V$  characteristics of an  $\alpha$ -In<sub>2</sub>Se<sub>3</sub> asymmetric c-FSJ during endurance measurement with  $V_{\text{Set/Reset}} = \pm 5$  V up to  $10^6$  cycles. Figure 4(d) shows the endurance characteristics measured at 0.2 V with  $V_{\text{Set/Reset}} = \pm 5$  V, which is extracted from  $I$ – $V$  sweep measurements. An endurance greater than  $10^6$  cycles is achieved at  $V_{\text{Set/Reset}} = \pm 5$  V.

The above results demonstrate that a higher on/off ratio can be achieved by introducing asymmetry in the FSJ structure. Here, an alternate asymmetric structure is proposed and also experimentally demonstrated, as shown in Figure 5(a), with a thin layer of Al<sub>2</sub>O<sub>3</sub> inserted between  $\alpha$ -In<sub>2</sub>Se<sub>3</sub> and one metal electrode to form a metal/ $\alpha$ -In<sub>2</sub>Se<sub>3</sub>/insulator/metal structure. The thickness of the Al<sub>2</sub>O<sub>3</sub> is well controlled by atomic layer deposition (ALD) to modulate the band bending in In<sub>2</sub>Se<sub>3</sub>, as shown in Figure 5(b). The depletion region in  $\alpha$ -In<sub>2</sub>Se<sub>3</sub> formed at the  $\alpha$ -In<sub>2</sub>Se<sub>3</sub>/Al<sub>2</sub>O<sub>3</sub> interface determines  $\Phi_{\text{eff}}$ , thus resulting in low and high resistances in the on- and off-states. The electron transport mechanism is similar to the metal/ $\alpha$ -In<sub>2</sub>Se<sub>3</sub>/Si structure. However, it is easier to engineer the asymmetry by

the accurate thickness control of the Al<sub>2</sub>O<sub>3</sub> interfacial layer by ALD. The  $I$ – $V$  characteristics of the  $\alpha$ -In<sub>2</sub>Se<sub>3</sub> c-FSJ with different Al<sub>2</sub>O<sub>3</sub> interfacial layer thicknesses are presented in Figure 5(c). As can be seen, the on/off ratio is enhanced significantly from  $\sim 10^2$  to  $>10^8$  as the thickness of the Al<sub>2</sub>O<sub>3</sub> interfacial layer increases from 1 nm to 4 nm. Meanwhile, a thicker Al<sub>2</sub>O<sub>3</sub> interfacial layer leads to larger coercive voltages because of the additional voltage drop across Al<sub>2</sub>O<sub>3</sub>. These results confirm that introducing stronger asymmetry contributes to the enhancement of the on/off ratio of the FSJs. Note that the electron tunneling through the insulator layer here may result in the degradation of endurance, as shown in the retention and endurance measurement in Figure S3. Therefore, for practical applications, a metal/ $\alpha$ -In<sub>2</sub>Se<sub>3</sub>/Si asymmetric c-FSJ could be a more preferred structure.

## CONCLUSIONS

In conclusion, an asymmetric metal/ $\alpha$ -In<sub>2</sub>Se<sub>3</sub>/Si c-FSJ is proposed and experimentally demonstrated. A high-performance  $\alpha$ -In<sub>2</sub>Se<sub>3</sub> c-FSJ is achieved taking advantage of the essential asymmetry provided by the depletion in doped silicon electrode, exhibiting a high on/off ratio  $> 10^4$  at room temperature, on/off ratio  $> 10^3$  at an elevated temperature of 140 °C, retention  $> 10^4$  s, and endurance  $> 10^6$  cycles. The on/off ratio of the asymmetric  $\alpha$ -In<sub>2</sub>Se<sub>3</sub> can be enhanced to  $>10^8$  by introducing a metal/ $\alpha$ -In<sub>2</sub>Se<sub>3</sub>/insulator/metal structure. These results suggest the  $\alpha$ -In<sub>2</sub>Se<sub>3</sub> c-FSJ is a promising ferroelectric device candidate for low-power high-density nonvolatile memory and neuromorphic computing applications.

## METHODS

**Device Fabrication.** The device fabrication started with atomic layer deposition of 15 nm  $\text{Al}_2\text{O}_3$  on top of the p+ Si substrate, using trimethylaluminum (TMA) and water as Al and O precursors at 175 °C. The bottom electrode was patterned by photolithography, and an  $\text{Al}_2\text{O}_3$  trench was etched by buffered oxide etch (BOE) solution to expose the p+ Si bottom electrode. Then, mechanically exfoliated  $\alpha\text{-In}_2\text{Se}_3$  was transferred on top of the trench, followed by e-beam evaporation of the Ni/Au top electrode.  $\alpha\text{-In}_2\text{Se}_3$  was grown by the chemical vapor transport (CVT) method itself.

**Device Characterization.** The thickness of the  $\text{In}_2\text{Se}_3$  was measured using a Veeco Dimension 3100 atomic force microscope (AFM) system. Electrical characterization was carried out with a Keysight B1500 system in a Cascade Summit probe station.

## ASSOCIATED CONTENT

## Supporting Information

The Supporting Information is available free of charge at <https://pubs.acs.org/doi/10.1021/acsnano.1c00968>.

Additional details for the wake-up effects, thickness dependences on the asymmetric  $\text{In}_2\text{Se}_3$  FSJs, and retention and endurance of metal/ $\alpha\text{-In}_2\text{Se}_3$ /insulator/metal c-FSJ (PDF)

## AUTHOR INFORMATION

## Corresponding Author

Peide D. Ye – School of Electrical and Computer Engineering and Birck Nanotechnology Center, Purdue University, West Lafayette, Indiana 47907, United States; [orcid.org/0000-0001-8466-9745](https://orcid.org/0000-0001-8466-9745); Email: [yep@purdue.edu](mailto:yep@purdue.edu)

## Authors

Mengwei Si – School of Electrical and Computer Engineering and Birck Nanotechnology Center, Purdue University, West Lafayette, Indiana 47907, United States; [orcid.org/0000-0003-0397-7741](https://orcid.org/0000-0003-0397-7741)

Zhuocheng Zhang – School of Electrical and Computer Engineering and Birck Nanotechnology Center, Purdue University, West Lafayette, Indiana 47907, United States

Sou-Chi Chang – Components Research, Intel Corporation, Hillsboro, Oregon 97124, United States

Nazila Haratipour – Components Research, Intel Corporation, Hillsboro, Oregon 97124, United States

Dongqi Zheng – School of Electrical and Computer Engineering and Birck Nanotechnology Center, Purdue University, West Lafayette, Indiana 47907, United States

Junkang Li – School of Electrical and Computer Engineering and Birck Nanotechnology Center, Purdue University, West Lafayette, Indiana 47907, United States

Uygar E. Avci – Components Research, Intel Corporation, Hillsboro, Oregon 97124, United States

Complete contact information is available at: <https://pubs.acs.org/doi/10.1021/acsnano.1c00968>

## Author Contributions

P.D.Y. and M.S. conceived the idea and proposed the asymmetric crossbar ferroelectric semiconductor junction. M.S., Z.Z., and D.Z. did the device fabrication. M.S. and Z.Z. performed DC electrical and temperature-dependent measurements and analysis. M.S., J.L., and Z.Z. did endurance and retention measurements. S.C.C., N.H., and U.E.A. did the device modeling. M.S., Z.Z., and P.D.Y. cowrote the manuscript, and all authors commented on it.

## Notes

The authors declare no competing financial interest.

## ACKNOWLEDGMENTS

The authors would like to thank A. K. Saha and S. K. Gupta for valuable discussions and J. K. Qin, J. Jian, and H. Wang for the technical support on TEM imaging. The work was supported by Intel Corporation.

## REFERENCES

- (1) Akinaga, H.; Shima, H. Resistive Random Access Memory (ReRAM) Based on Metal Oxides. *Proc. IEEE* **2010**, *98*, 2237–2251.
- (2) Yang, J. J.; Strukov, D. B.; Stewart, D. R. Memristive Devices for Computing. *Nat. Nanotechnol.* **2013**, *8*, 13–24.
- (3) Wong, H.-S. P.; Raoux, S.; Kim, S.; Liang, J.; Reifenberg, J. P.; Rajendran, B.; Asheghi, M.; Goodson, K. E. Phase Change Memory. *Proc. IEEE* **2010**, *98*, 2201–2227.
- (4) Pantel, D.; Goetze, S.; Hesse, D.; Alexe, M. Room-Temperature Ferroelectric Resistive Switching in Ultrathin  $\text{Pb}(\text{Zr}_{0.2}\text{Ti}_{0.8})\text{O}_3$  Films. *ACS Nano* **2011**, *5*, 6032–6038.
- (5) Chanthbouala, A.; Crassous, A.; Garcia, V.; Bouzouhane, K.; Fusil, S.; Moya, X.; Allibe, J.; Dlubak, B.; Grollier, J.; Xavier, S.; Deranlot, C.; Moshar, A.; Proksch, R.; Mathur, N. D.; Bibes, M.; Barthélémy, A. Solid-State Memories Based on Ferroelectric Tunnel Junctions. *Nat. Nanotechnol.* **2012**, *7*, 101–104.
- (6) Chanthbouala, A.; Garcia, V.; Cherifi, R. O.; Bouzouhane, K.; Fusil, S.; Moya, X.; Xavier, S.; Yamada, H.; Deranlot, C.; Mathur, N. D.; Bibes, M.; Barthélémy, A.; Grollier, J. A Ferroelectric Memristor. *Nat. Mater.* **2012**, *11*, 860–864.
- (7) Yamada, H.; Garcia, V.; Fusil, S.; Boyn, S.; Marinova, M.; Gloter, A.; Xavier, S.; Grollier, J.; Jacquet, E.; Carrétero, C.; Deranlot, C.; Bibes, M.; Barthélémy, A. Giant Electroresistance of Super-Tetragonal  $\text{BiFeO}_3$ -Based Ferroelectric Tunnel Junctions. *ACS Nano* **2013**, *7*, 5385–5390.
- (8) Wen, Z.; Li, C.; Wu, D.; Li, A.; Ming, N. Ferroelectric-Field-Effect-Enhanced Electroresistance in Metal/Ferroelectric/Semiconductor Tunnel Junctions. *Nat. Mater.* **2013**, *12*, 617–621.
- (9) Garcia, V.; Bibes, M. Ferroelectric Tunnel Junctions for Information Storage and Processing. *Nat. Commun.* **2014**, *5*, 4289.
- (10) Fujii, S.; Kamimuta, Y.; Ino, T.; Nakasaki, Y.; Takashi, R.; Saitoh, M. First Demonstration and Performance Improvement of Ferroelectric  $\text{HfO}_2$ -Based Resistive Switch with Low Operation Current and Intrinsic Diode Property. In *2016 IEEE Symposium on VLSI Technology*; IEEE, 2016; pp 1, 2.
- (11) Xi, Z.; Ruan, J.; Li, C.; Zheng, C.; Wen, Z.; Dai, J.; Li, A.; Wu, D. Giant Tunneling Electroresistance in Metal/Ferroelectric/Semiconductor Tunnel Junctions by Engineering the Schottky Barrier. *Nat. Commun.* **2017**, *8*, 1–9.
- (12) Wurfel, P.; Batra, I. P. Depolarization-Field-Induced Instability in Thin Ferroelectric Films—Experiment and Theory. *Phys. Rev. B* **1973**, *8*, 5126–5133.
- (13) Ma, T. P.; Han, J. P. Why Is Nonvolatile Ferroelectric Memory Field-Effect Transistor Still Elusive? *IEEE Electron Device Lett.* **2002**, *23*, 386–388.
- (14) Tian, X.; Shibayama, S.; Nishimura, T.; Yajima, T.; Migita, S.; Toriumi, A. Evolution of Ferroelectric  $\text{HfO}_2$  in Ultrathin Region down to 3 nm. *Appl. Phys. Lett.* **2018**, *112*, 102902.
- (15) Lyu, X.; Si, M.; Sun, X.; Capano, M. A.; Wang, H.; Ye, P. D. Ferroelectric and Anti-Ferroelectric Hafnium Zirconium Oxide: Scaling Limit, Switching Speed and Record High Polarization Density. In *2019 Symposium on VLSI Technology*; IEEE, 2019; pp T44, T45.
- (16) Xue, F.; He, X.; Retamal, J. R. D.; Han, A.; Zhang, J.; Liu, Z.; Huang, J.; Hu, W.; Tung, V.; He, J.; Li, L.; Zhang, X. Gate-Tunable and Multidirection-Switchable Memristive Phenomena in a Van der Waals Ferroelectric. *Adv. Mater.* **2019**, *31*, 1901300.
- (17) Si, M.; Luo, Y.; Chung, W.; Bae, H.; Zheng, D.; Li, J.; Qin, J.; Qiu, G.; Yu, S.; Ye, P. D. A Novel Scalable Energy-Efficient Synaptic Device: Crossbar Ferroelectric Semiconductor Junction. In *2019 IEEE*

*International Electron Devices Meeting (IEDM)*; IEEE, 2019; pp 130–133.

(18) Jerry, M.; Chen, P.-Y.; Zhang, J.; Sharma, P.; Ni, K.; Yu, S.; Datta, S. Ferroelectric FET Analog Synapse for Acceleration of Deep Neural Network Training. In *2017 IEEE International Electron Devices Meeting (IEDM)*; IEEE, 2017; pp 139–142.

(19) Chung, W.; Si, M.; Ye, P. D. First Demonstration of Ge Ferroelectric Nanowire FET as Synaptic Device for Online Learning in Neural Network with High Number of Conductance State and  $G_{\text{Max}}/G_{\text{Min}}$ . In *2018 IEEE International Electron Devices Meeting (IEDM)*; IEEE, 2018; pp 344–347.

(20) Si, M.; Saha, A. K.; Gao, S.; Qiu, G.; Qin, J.; Duan, Y.; Jian, J.; Niu, C.; Wang, H.; Wu, W.; Gupta, S. K.; Ye, P. D. A Ferroelectric Semiconductor Field-Effect Transistor. *Nat. Electron.* **2019**, *2*, 580–586.

(21) Ding, W.; Zhu, J.; Wang, Z.; Gao, Y.; Xiao, D.; Gu, Y.; Zhang, Z.; Zhu, W. Prediction of Intrinsic Two-Dimensional Ferroelectrics in  $\text{In}_2\text{Se}_3$  and Other III<sub>2</sub>-VI<sub>3</sub> van der Waals Materials. *Nat. Commun.* **2017**, *8*, 14956.

(22) Poh, S. M.; Tan, S. J. R.; Wang, H.; Song, P.; Abidi, I. H.; Zhao, X.; Dan, J.; Chen, J.; Luo, Z.; Pennycook, S. J.; Castro Neto, A. H.; Loh, K. P. Molecular-Beam Epitaxy of Two-Dimensional  $\text{In}_2\text{Se}_3$  and Its Giant Electroresistance Switching in Ferroresistive Memory Junction. *Nano Lett.* **2018**, *18*, 6340–6346.

(23) Zheng, C.; Yu, L.; Zhu, L.; Collins, J. L.; Kim, D.; Lou, Y.; Xu, C.; Li, M.; Wei, Z.; Zhang, Y.; Edmonds, M. T.; Li, S. Room Temperature In-Plane Ferroelectricity in van der Waals  $\text{In}_2\text{Se}_3$ . *Sci. Adv.* **2018**, *4*, eaar7720.

(24) Xiao, J.; Zhu, H.; Wang, Y.; Feng, W.; Hu, C.; Dasgupta, A.; Han, Y.; Wang, Y.; Muller, D. A.; Martin, L. W.; Hu, P.; Zhang, X. Intrinsic Two-Dimensional Ferroelectricity with Dipole Locking. *Phys. Rev. Lett.* **2018**, *120*, 227601.

(25) Cui, C.; Hu, W.; Yan, X.; Addiego, C.; Gao, W.; Wang, Y.; Wang, Z.; Li, L.; Cheng, Y.; Li, P.; Zhang, X.; Alshareef, H. N.; Wu, T.; Zhu, W.; Pan, X.; Li, L.-J. Intercorrelated In-Plane and Out-of-Plane Ferroelectricity in Ultrathin Two-Dimensional Layered Semiconductor  $\text{In}_2\text{Se}_3$ . *Nano Lett.* **2018**, *18*, 1253–1258.

(26) Xue, F.; Hu, W.; Lee, K.; Lu, L.; Zhang, J.; Tang, H.; Han, A.; Hsu, W.; Tu, S.; Chang, W.; Lien, C.; He, J. Room-Temperature Ferroelectricity in Hexagonally Layered  $\alpha\text{-In}_2\text{Se}_3$  Nanoflakes down to the Monolayer Limit. *Adv. Funct. Mater.* **2018**, *28*, 1803738.

(27) Sze, S. M.; Ng, K. K. *Physics of Semiconductor Devices*, 3rd ed.; John Wiley & Sons: Hoboken, NJ, 2006.